nature microbiology

Article

https://doi.org/10.1038/s41564-022-01243-4

Bacteriophage genome engineering with CRISPR–Cas13a

Received: 25 February 2022

Accepted: 2 September 2022

Published online: 31 October 2022

Check for updates

Jingwen Guan[1], Agnès Oromí-Bosch[2], Senén D. Mendoza[1,5], Shweta Karambelkar[1], Joel D. Berry[2] and Joseph Bondy-Denomy[1,3,4]

Jumbo phages such as *Pseudomonas aeruginosa* ΦKZ have potential as antimicrobials and as a model for uncovering basic phage biology. Both pursuits are currently limited by a lack of genetic engineering tools due to a proteinaceous 'phage nucleus' structure that protects from DNA-targeting CRISPR–Cas tools. To provide reverse-genetics tools for DNA jumbo phages from this family, we combined homologous recombination with an RNA-targeting CRISPR–Cas13a enzyme and used an anti-CRISPR gene (*acrVIA1*) as a selectable marker. We showed that this process can insert foreign genes, delete genes and add fluorescent tags to genes in the ΦKZ genome. Fluorescent tagging of endogenous gp93 revealed that it is ejected with the phage DNA while deletion of the tubulin-like protein PhuZ surprisingly had only a modest impact on phage burst size. Editing of two other phages that resist DNA-targeting CRISPR–Cas systems was also achieved. RNA-targeting Cas13a holds great promise for becoming a universal genetic editing tool for intractable phages, enabling the systematic study of phage genes of unknown function.

Bacteriophages infect bacteria and can cause cell lysis after replication. In recent decades, the rapid emergence of multidrug-resistant bacterial pathogens and simultaneous decline in the discovery of antibiotics has rekindled interest in the use of phages as alternative antimicrobial therapeutics (phage therapy)[1,2]. Phages offer many advantages over antibiotics, including high specificity and efficient propagation in the presence of their bacterial host[3–5]. However, host range limitations and the rapid emergence of phage resistance in clinical strains present barriers to the adoption of phage therapy[1,3,6]. Phage genome engineering might help to overcome these hurdles[7,8]. Robust phage engineering tools could aid fundamental discoveries, broaden host range, enhance evasion of host antiviral defence systems and reduce phage immunogenicity[9–12]. Phage engineering techniques often include homologous recombination with a template plasmid[13,14], coupled with a selective pressure, such as CRISPR–Cas targeting. CRISPR–Cas systems (that is, clustered regularly interspaced short palindromic repeats and CRISPR-associated proteins) are adaptive anti-phage immune systems in prokaryotes[15,16]. CRISPR–Cas programmable targeting enables effective enrichment for phage recombinants by removing wild-type (WT) phages from the population and has been coupled with the integration of an anti-CRISPR gene as a selectable marker[17].

To date, all CRISPR-based screening tools used in phage engineering recognize and target phage genomic DNA. However, phages have evolved a multitude of strategies to circumvent DNA-targeting immunity, including anti-CRISPR proteins, DNA base modifications and genome segregation[18,19]. The *Pseudomonas aeruginosa* jumbo phage ΦKZ is resistant to a broad range of DNA-targeting immune systems via assembly of a proteinaceous 'phage nucleus' structure that shields phage DNA during replication[20,21]. Therefore, this phage family is a good candidate for use as a phage therapeutic but no genetic tools are available for jumbo phages and most basic biology studies of this phage family have relied on plasmid-based overexpression of jumbo phage genes[22].

Although the phage nucleus protects phage DNA from being targeted by bacterial immune defences, the messenger RNA-targeting CRISPR–Cas13a system (type VI-A)[23] effectively inhibits ΦKZ replication by degrading phage mRNA that is exported from the phage

[1]Department of Microbiology & Immunology, University of California, San Francisco, CA, USA. [2]Felix Biotechnology, Inc., San Francisco, CA, USA. [3]Quantitative Biosciences Institute, University of California, San Francisco, CA, USA. [4]Innovative Genomics Institute, Berkeley, CA, USA. [5]Present address: Department of Biology, Massachusetts Institute of Technology, Cambridge, MA, USA. e-mail: joseph.bondy-denomy@ucsf.edu

nucleus to the cytoplasm[20]. The promiscuous cleavage of bacterial and phage transcripts by activated Cas13a limits the emergence of CRISPR-resistant escape phages[24] and may aid the identification of engineered mutant phages.

We report the development of a CRISPR–Cas13a system as a genetic engineering method for ΦKZ. Using Cas13a to target an essential transcript, we selected for phages that have undergone homologous recombination resulting in a desired genetic change along with the acquisition of an anti-Cas13a *trans* gene, *acrVIA1* (derived from Listeriophage ΦLS46 (ref. [25])), as a selectable marker. This approach allowed us to precisely insert foreign gene fragments into the ΦKZ genome, knock out non-essential genes and fuse fluorescent tags to individual genes. Importantly, the same guide can be used for any genomic manipulation since engineered phages are identified based on the acquisition of the Cas13a inhibitor, not a change in the target sequence. Our work establishes a Cas13a-based phage engineering strategy that could be universally applied for engineering phages.

Results

Optimization of CRISPR–Cas13a for efficient phage targeting

Cas13a is an RNA-guided RNA nuclease that can block ΦKZ replication in *P. aeruginosa* PAO1. We previously targeted ΦKZ by expressing LseCas13a (derived from *Listeria seeligeri*) from the PAO1 chromosome under a pLac inducible promoter and CRISPR-derived RNA (crRNA) guides from a plasmid (Fig. 1a, V1)[20]. We selected LseCas13a because of its prior thorough biochemical characterization[23,26,27]. For the effective elimination of WT phages in the population, we first sought to enhance the activity of crRNA guides. We designed version 2 (V2) with the repeat-spacer-repeat unit moved to the +1 transcription start site of the P_{BAD} promoter and the second direct repeat mutated to remove repeat homology (Fig. 1a). To further stabilize the crRNA cassette, we next omitted the second direct repeat and generated V3 (Fig. 1a), which could prevent recombination between the repeats. Using the same spacer, both V2 and V3 provided more robust defence against phage JBD30 and ΦKZ compared with V1 (Fig. 1a). For simplicity, we selected the V3 cassette, which has a single repeat to express crRNAs against ΦKZ. We designed guides with 24 nucleotide spacers complementary to randomly selected regions of various ΦKZ gene transcripts. Strong targeting was observed for some crRNAs, to the point that mutant escape phages could be isolated, such as the two spacers matching the *orf120* and *orf146* transcripts, but not all crRNAs were efficacious (Extended Data Fig. 1). Given the variability of targeting efficiency, for the remainder of this article, we use the crRNA targeting the ΦKZ *orf120* transcripts (Extended Data Fig. 1) as our primary guide to screen for engineered phages. We refer the PAO1 strain simultaneously expressing Cas13a and *orf120*-crRNA to as the Cas13a counterselection strain. We describe below how the same guide can be used to facilitate the engineering of distinct genomic loci.

Isolation of ΦKZ recombinants by CRISPR–Cas13a selection

To avoid disrupting any essential genes that are required for phage replication, we first attempted to insert *acrVIA1* immediately downstream of the ΦKZ major capsid gene (*orf120*). A template DNA substrate for homologous recombination, composed of approximately 600 base pair (bp) homology arms flanking *acrVIA1* (669 bp) plus a 30 bp sequence including Shine–Dalgarno site was cloned into a plasmid, referred to as an editing plasmid (Fig. 1b). After infecting a PAO1 strain possessing the editing plasmid to allow recombination, the phage lysate was then titrated on a lawn of the Cas13a counterselection strain to eliminate WT phages. To screen for recombinants, individual plaques were examined for *acrVIA1* integration via PCR using two sets of primers to confirm integration of *acrVIA1* at the correct locus (Fig. 1b). This approach resulted in the isolation of recombinants (Fig. 1c,d). Sanger sequencing further confirmed the correct genomic integration junction. Recombinant phages propagated well on hosts expressing crRNAs targeting other transcripts due to the expression of *acrVIA1* (Fig. 1e), which abolishes Cas13a immunity regardless of the crRNA sequence. Recombinant phages formed plaques on PAO1 with a similar size and efficiency compared to WT phages and phage latent periods and burst sizes were unaffected (Extended Data Fig. 2). This demonstrated that the insertion did not cause a fitness defect. Three randomly selected plaques that escaped Cas13a targeting but screened negative for the *acrVIA1* integration contained genomic deletions ranging from 27 to 69 bp starting immediately downstream of the *orf120* stop codon, disrupting the protospacer (Extended Data Fig. 3). Therefore, while the crRNA used is not inescapable, the recombination efficiency to insert the selectable marker is clearly efficient enough to enable facile identification of the desired mutants.

To test the flexibility of this nascent genetic technology (Fig. 1f) and generate new biological insights of phage ΦKZ, we next replaced (or attempted to replace) multiple genes with *acrVIA1* (results summarized in Table 1), *phuZ* (*orf39*, tubulin homologue), *orf54* (major shell/nucleus protein), *orf89–orf93* (inner body proteins), *orf93*, *orf146* (tail protein), *orf241* and *orf241–orf242* (small accessory proteins), in addition to attempting to add fluorescent tags onto *phuZ, orf54* and *orf93* in the phage genome. The successes, failures and new insights gained are discussed below. Whole genome sequencing (WGS) of two deletion mutants, *phuZ::acrVIA1* and *orf93::acrVIA1*, revealed no other mutations, highlighting the accuracy of this RNA-targeting system to select for the desired changes in DNA phage genomes.

Characterization of PhuZ and gp93 using engineered ΦKZ

PhuZ (gp39) is a tubulin homologue conserved across many jumbo phages and some megaphages[28,29]. It assembles a bipolar spindle to centre the phage nucleus during phage intracellular development[30,31] and 'treadmill' newly synthesized phage capsids from the cell inner membrane to the phage nucleus for DNA packaging[32]. These roles made us speculate that PhuZ might be essential for phage growth; however, this is not the case. *phuZ::acrVIA1* (herein, Δ*phuZ*) mutants formed plaques on a PAO1 lawn that were indistinguishable from WT plaques and exhibited a similar latent period (approximately 60 min) compared with WT phages (Extended Data Fig. 2). However, burst size significantly decreased (15 phage particles per infected bacterial cell on average versus 39 of the WT phages) (Extended Data Fig. 2). While cells infected with WT phages or *ΔphuZ* mutants complemented *in trans* had phage nuclei in the centre of the cell approximately 80% of the time, the localization of the phage nucleus showed a wide distribution in cells infected by Δ*phuZ* mutants (Fig. 2a,b and Supplementary Video 1). This is consistent with the previous findings that *trans* overexpression of catalytic mutant PhuZ resulted in mispositioning of the phage nucleus[31,33]. Approximately 25% of mutant-infected cells still positioned the phage nucleus at the cell centre (Fig. 2b), a phenotype most commonly seen in shorter cells (Pearson correlation coefficient = 0.486, $P < 0.001$), in contrast with WT infection where no correlation was observed with cell size (Pearson correlation coefficient = 0.029, $P = 0.505$) (Fig. 2c). Considering that PhuZ is proposed to traffic phage capsids from the cell inner membrane to the phage nucleus[32,34] but is apparently non essential, we speculate that this trafficking is only required under unidentified conditions or not at all. Taken together, these data confirm that PhuZ is required for the consistent positioning of the phage nucleus at the cell centre during infection; however, its removal and the subsequent mislocalization of the phage nucleus, do not abolish phage replication under laboratory conditions.

Orf93 encodes gp93, a high copy number 'inner body' protein that is packaged in the phage head[35,36]. Replacement of *orf93* with *acrVIA1* (*orf93::acrVIA1*, herein Δ*orf93*) also yielded a viable phage that generated plaques with similar size and efficiency. To assess whether the loss of *phuZ* or *orf93* would impact growth in a strain-dependent manner, we challenged a panel of 21 *P. aeruginosa* clinical strains with the mutant phages. Plaque assays showed that host ranges and

https://doi.org/10.1038/s41564-022-01243-4

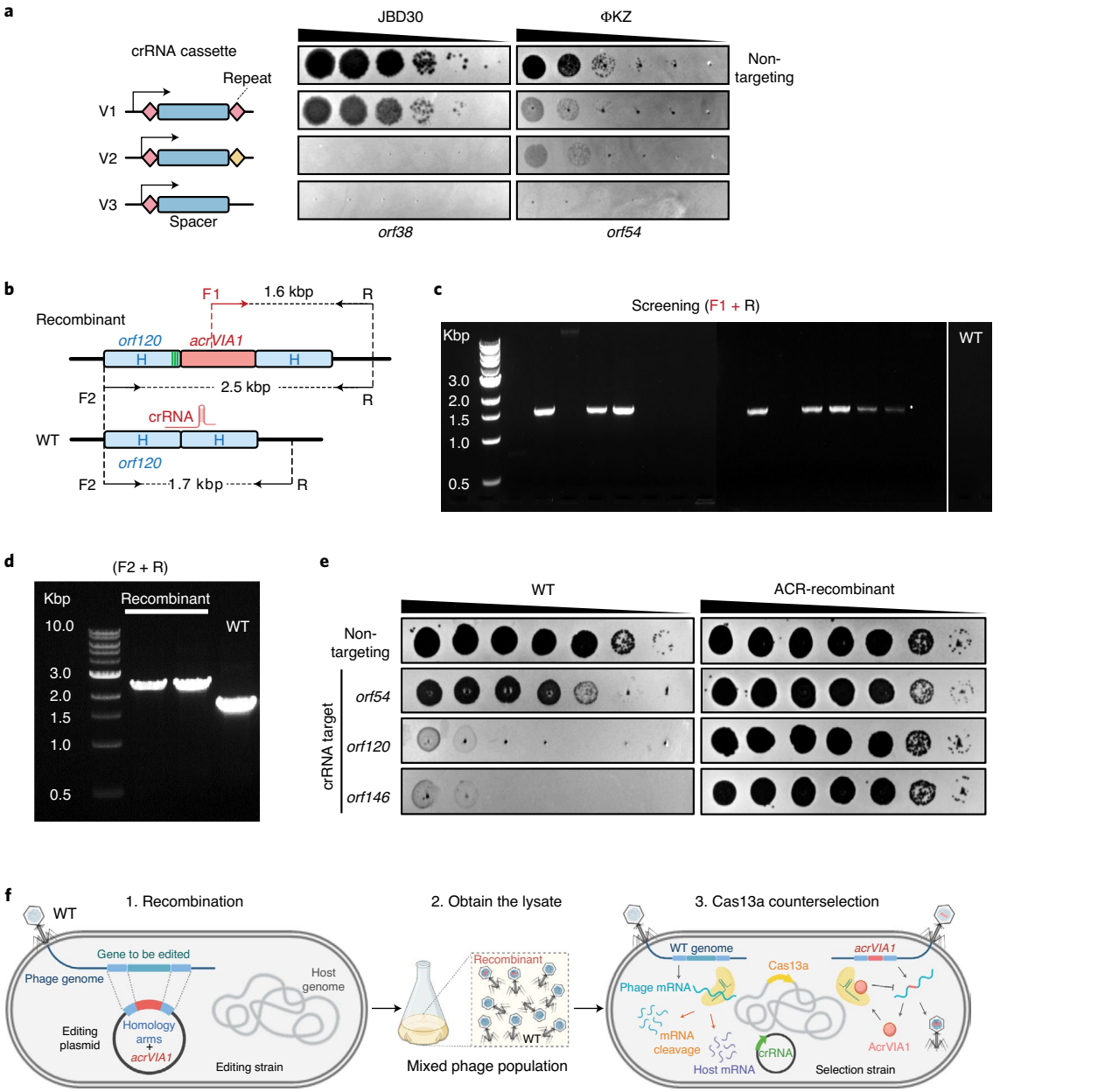

Fig. 1 | Screening for ΦKZ recombinants by CRISPR–Cas13a counter selection. a, Schematic of three versions of the CRISPR–Cas13a crRNA cassette and their efficiency of plating assays targeting two unrelated phages: JBD30 and ΦKZ. Spacers are represented by dark blue rectangles. Repeats are shown as diamonds with different colours (pink and yellow) indicating different repeat sequences. The arrows represent the transcription start sites of the P_{BAD} promoter. The cassettes carried the same spacer sequences targeting the transcripts of *orf38* of JBD30 and *orf54* of ΦKZ, respectively. **b**, Schematic of WT ΦKZ and recombinant genomes at the editing site. The *acrVIA1* gene, shown as a red rectangle, was inserted downstream of *orf120*, with upstream and downstream of the homology (H) arms indicated by the light blue rectangles. The green stripes represent synonymous mutations that were introduced to the homology region in only this case. Synonymous mutations were not necessary because of the effectiveness of the AcrVIA1 marker on the inhibition of Cas13a activities. F and R indicate forward and reverse primers, respectively, used to confirm the insertion of *acrVIA1*. **c**, Recombinant phages were screened by PCR using the F1 and R primers. **d**, PCR using the F2 and R primers with purified recombinant phage plaques. Expected sizes: 1.7 kbp for WT and 2.5 kbp for recombinants. **e**, Ten-fold serial dilutions of WT or an *acrVIA1* recombinant phage spotted on lawns of cells expressing *cas13* and three different crRNAs targeting the indicated phage genes along with a non-targeting control. PCR-based mutant screening, and the subsequent plaque assays, were independently repeated three times yielding similar results. **f**, Workflow of phage genome engineering using CRISPR–Cas13a. (1) An editing plasmid introduces the desired genetic modifications via recombination. (2) A mixed phage lysate is generated. (3) The lysate is plated on the selection strain harbouring Cas13a and a crRNA targeting WT phages.

plaque morphologies of both mutants were quite similar to WT (Fig. 2d and Extended Data Fig. 4), suggesting that these knockouts, and Cas13a-mediated genetic engineering in general, have no impact on the ΦKZ host range.

We next inserted a fluorescent label at the C terminus of gp93 (Fig. 3a), which is notable as the first genomic protein tag in this phage family. This was again achieved with the *acrVIA1* selectable marker (Fig. 3a). Labelled gp93 was observed in the mature virion (Fig. 3a), as predicted by previous mass spectrometry studies[36]. Excitingly, time-lapse videos revealed the fluorescently labelled protein being injected with the phage DNA at the cell pole (Fig. 3b and Supplementary Video 2) and subsequently translocating to the cell centre where

https://doi.org/10.1038/s41564-022-01243-4

Table 1 | Summary of phage mutants engineered by CRISPR–Cas13a

Phage	Gene number/genomic site	Identified protein	Modification	Percentage plaques *acrVIA1*+[a] (*n*)[b]	Desired mutant isolated?
ΦKZ	Upstream of *orf54*	–	Insertion	41.2% (17)	Yes
	Downstream of *orf120*	–	Insertion	50.0% (16)	
	orf39	PhuZ	Deletion	52.9% (17)	
			mNeonGreen-PhuZ fusion	25.0% (16)	
			mCherry-PhuZ fusion	25.0% (16)	
	orf93	Inner body protein	Deletion	20.0% (20)	
			gp93-mNeonGreen fusion	18.2% (22)	
	orf241	Hypothetical	Deletion	26.1% (23)	
	orf241, *orf242*	Hypothetical	Double deletion	41.7% (12)	
	orf54	Shell	Deletion	20.0% (15)	No
			mCherry-gp54 fusion	8.3% (24)	
			gp54-mCherry fusion	9.1% (11)	
			gfp11-gp54 fusion	7.0% (57)	
	orf89–orf93	Inner body proteins	Deletion	11.8% (17)	
	orf146	Structural protein	Deletion	0% (89)	
OMKO1	Downstream of the capsid gene	–	Insertion with a barcode	70.8% (24)	Yes
	Upstream of the shell gene	–	Insertion	50.0% (12)	
PaMx41	*orf24*	Hypothetical	Deletion	100.0% (8)	Yes

[a]Percentage of PCR-identified recombinants out of all tested plaques. [b]Number of plaques analysed by PCR to screen for recombinants.

it remained bound to the phage nucleus. As new gp93-mNeonGreen was expressed from the phage genome, more and more green signals concentrated on the surface of the phage nucleus, while some foci appeared near the cell inner membrane. Finally, cells lysed and released fluorescent phage progeny. To confirm that the protein that appears to be injected was not rapidly synthesized de novo, we monitored the infection behaviours of WT phages loaded with gp93-mNeonGreen expressed from a plasmid during phage production but where no new fluorescent protein could be made during infection (Fig. 3c and Supplementary Video 3). Similar to the engineered phage, phage particles were fluorescent, injected the labelled protein and the green focus migrated from the cell pole to the cell centre along with phage DNA on the surface of the phage nucleus until cell lysis. However, no new labelled protein synthesis was observed, as expected. Therefore, the inner body protein gp93 is not only packaged in the phage head but may also play a role during phage injection and subsequent maturation to the phage nucleus. Our new ability to endogenously label phage proteins, as demonstrated in this study, will be beneficial for characterizing ΦKZ virion and cell biology in the future. Using a similar approach, mNeonGreen or mCherry were fused to PhuZ in the phage genome (Table 1); however, no fluorescent PhuZ filaments were visible during infection. These fusions formed fluorescent filaments when expressed from a plasmid but not from the phage genome, perhaps due to low expression levels or other factors.

The phage nucleus is primarily composed of gp54 (ref. [31]). We were unable to knock out or fluorescently label *orf54*, even when WT gp54 was provided by expressing from a plasmid *in trans*. The primers used to amplify the region of editing generated multiple bands for both deletion and tag-addition mutant variants (Extended Data Fig. 5a,b). N- or C-terminal fusion of gp54 with mCherry tags yielded similar results. WGS of an isolated *orf54* '*pseudo* knockout' (that is, a plaque that grew under Cas13a selection) strain revealed that part of the editing plasmid was integrated upstream of *orf54*, while the *orf54* gene was left intact (Extended Data Fig. 5c). Interestingly, a gene cluster of nearly the same length as the integrated plasmid (approximately 7 kilobase pair (kbp), *orf206–216*) was missing in the mutant, probably due to a limitation of phage packaging capacity. These data suggested that natural gp54 produced from phages must be present to ensure phage viability. A similar attempt to delete the structural gene (*orf146*) and a cluster of inner body genes (*orf89–orf93*) also failed, while deletion of the small, hypervariable accessory genes *orf241* and *orf241–242* succeeded but yielded no change in plaque size or efficiency. These results highlighted that the CRISPR–Cas13a counterselection system is a strong and efficient phage genome engineering tool but the modification of phage essential genes is challenging.

Precise genome engineering of clinical phage OMKO1

We next explored the versatility of our phage engineering platform by editing the genome of a clinical jumbo phage. We selected OMKO1, a *P. aeruginosa* phage with an approximate 280 kbp genome that has 90.1% nucleotide sequence identity to ΦKZ. OMKO1 is a potentially ideally therapeutic phage since *P. aeruginosa* strains that evolve resistance to infection become sensitized to small-molecule antibiotics[37]. This phage has been used for phage therapy as emergency treatment for chronic infections caused by antibiotic-resistant *P. aeruginosa*[38] and it is currently being tested in a phase I/II clinical trial (CYstic Fibrosis bacterioPHage Study at Yale, https://clinicaltrials.gov/ct2/show/NCT04684641). With this phage, we tested whether we could insert 'DNA barcodes' without impacting host range for downstream clinical applications. Insertion of a DNA tracking signature into clinical phages would enable differentiation from naturally occurring phages during the manufacturing process and after administration to patients.

Two engineered OMKO1 strains were generated, one with *acrVIA1* and a 120 nucleotide barcode inserted downstream of the capsid gene, and another with *acrVIA1* integrated upstream of the shell gene (*orf54* homologue; Fig. 4a and Table 1). The presence of the desired inserts was confirmed with WGS of both OMKO1 engineered strains; no unintended genetic changes occurred. Moreover, both

https://doi.org/10.1038/s41564-022-01243-4

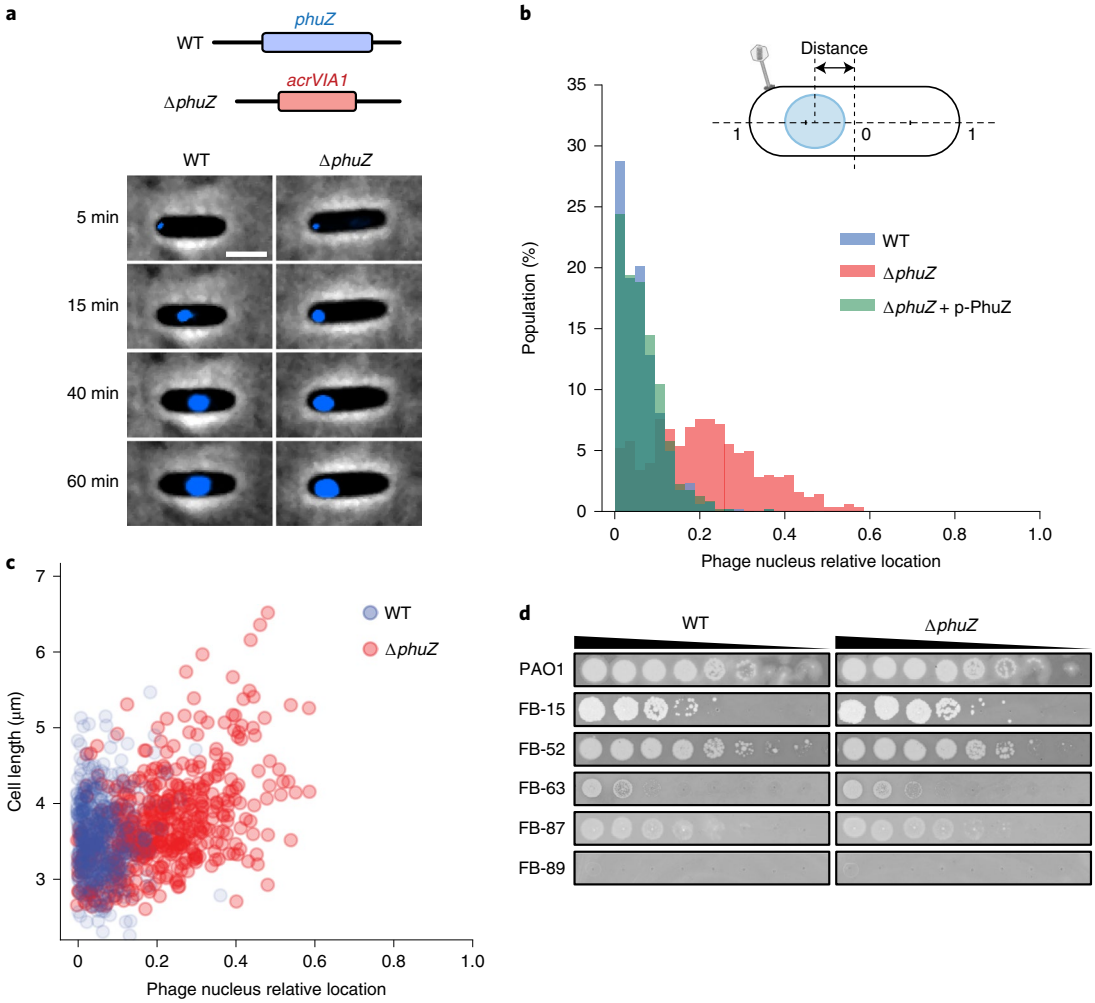

Fig. 2 | Absence of PhuZ causes mispositioning of the phage nucleus. a, Top: Schematic of ΦKZ WT and *phuZ*::*acrVIA1* (Δ*phuZ*) mutant genomes at the editing site. Bottom: Representative cells infected by WT (left) and Δ*phuZ* mutant (right). Phage DNA is stained with DAPI and shown as blue signals. Scale bar, 2 μm. **b**, Distribution of subcellular location of the phage nucleus in PAO1 cells infected by WT (blue, $n = 521$) and Δ*phuZ* (red, $n = 503$), and a PAO1 strain expressing WT PhuZ *in trans* (p-PhuZ) and infected by Δ*phuZ* (light green, $n = 573$). Top: Diagram of an infected cell. The phage nucleus location is defined as the relative distance between the cell centre and the nucleus centre. **c**, The phage nucleus location was plotted against the cell length for WT and Δ*phuZ*. Phage nucleus position in Δ*phuZ*-infected cells relative to cell size has a Pearson correlation coefficient of 0.486, $P < 0.001$ (two-sided), whereas WT infection has a Pearson correlation coefficient of 0.029, $P = 0.505$ (two-sided). **d**, Efficiency of plating WT and Δ*phuZ* on representative *P. aeruginosa* clinical strains. (The full panel of plaque assays is presented in Extended Data Fig. 4).

strains exhibited strong resistance to Cas13a targeting (Fig. 4b), owing to the expression of *acrVIA1* from the phage genomes. The host range and virulence of the two engineered OMKO1 variants together with the parental phage was then assessed on 22 *P. aeruginosa* clinical strains (including PAO1). The experiment was performed in a microplate liquid assay, where phage variants were individually mixed with each host strain at a multiplicity of infection (MOI) of approximately 1 and 0.01. All three phages displayed the same host range (Fig. 4c and Extended Data Fig. 6) and were capable of infecting and suppressing the growth of 20 out of 22 (91%) clinical strains tested. Infections at high MOI (MOI = 1) resulted in a broader host range and greater bacterial growth suppression, while low MOI (MOI = 0.01) infections suppressed the cell growth of 12 out of 22 (55%) hosts. All phages exhibited similar virulence across all hosts with small differences in 5 out of 22 strains (marked with an asterisk in Extended Data Fig. 6). Altogether, these results indicate that the OMKO1's host range was not affected and virulence was impacted only modestly by inserting *acrVIA1* or *acrVIA1* and a barcode in the two selected genome locations under the tested conditions.

CRISPR–Cas13a engineering of a lytic podophage

To evaluate the applicability of the CRISPR–Cas13a-mediated genome editing approach to other virulent phages, we selected the *P. aeruginosa* phage PaMx41. PaMx41 is a podophage (Genus: *Jamesmcgillvirus*) isolated from environmental and sewage water samples in Central Mexico[39]. Its genome is approximately 43.5 kbp long and harbours 55 open reading frames, approximately 70% of which have unknown function[40]. Remarkably, we discovered that PaMx41 appears to be resistant to many DNA-targeting CRISPR–Cas systems (type I-C, II-A and V-A) and showed partial sensitivity (approximately tenfold reduction in efficiency of plating) to type I-F to a degree that is not sufficient for counterselection (Fig. 5a). In contrast, when the transcripts of the major capsid gene (*orf11*) were targeted by CRISPR–Cas13a, PaMx41 exhibited strong sensitivities to specific crRNAs (Fig. 5b). Following the same approach as we developed to engineer ΦKZ, we successfully substituted one hypothetical gene (*orf24*) and its downstream non-coding region with *acrVIA1* and isolated a pure mutant strain using an efficient crRNA (no. 5, approximately 100-fold reduction in efficiency of plating) (Fig. 5b and Table 1). The mutant showed expected anti-CRISPR

https://doi.org/10.1038/s41564-022-01243-4

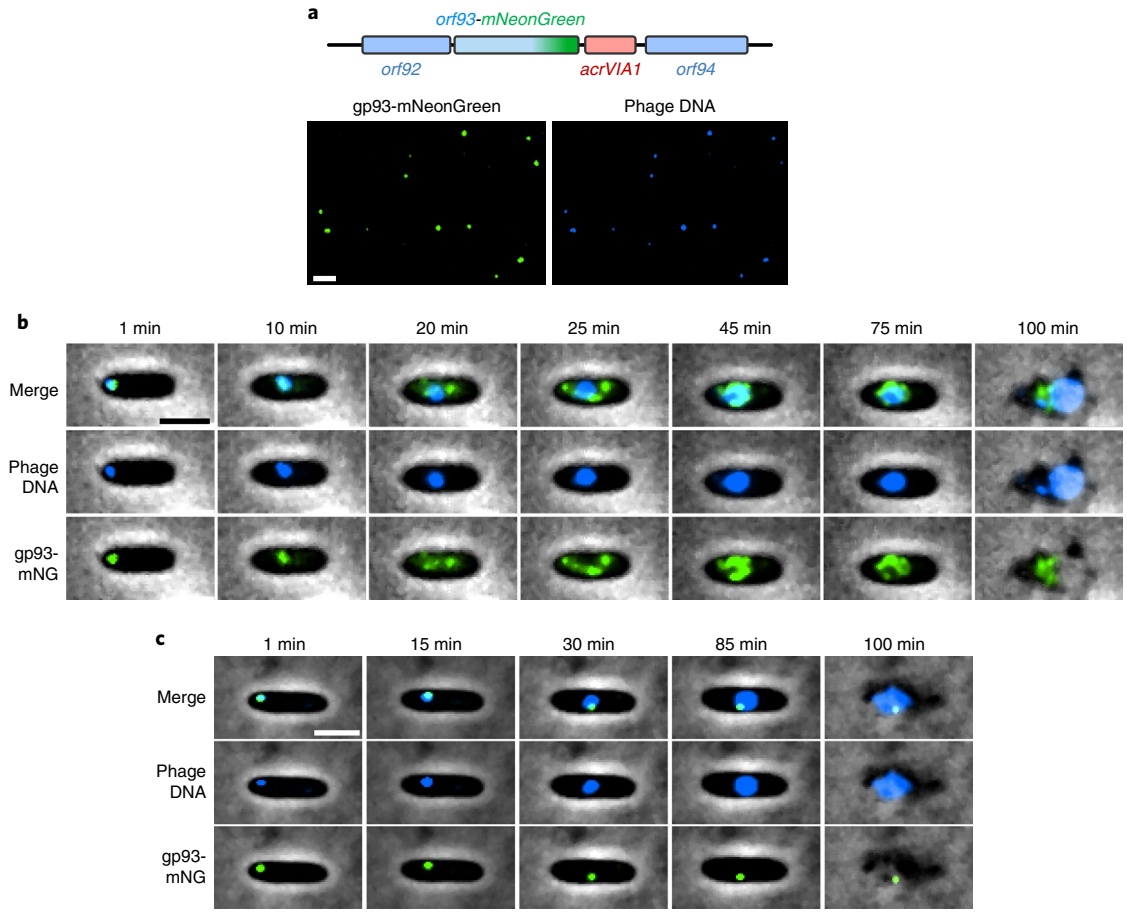

Fig. 3 | Fluorescent labelling of an inner body protein of ΦKZ. a, Top: Schematic of the ΦKZ *orf93-mNeonGreen* mutant at the editing site. The *acrVIA1* gene was inserted downstream of the *orf93-mNeonGreen* fusion cassette. Bottom: Visualization of individual phage particles under a fluorescence microscope. Each mutant phage particle is visible as a green focus (left) due to the packaging of gp93-mNeonGreen in the capsid. ΦKZ genomic DNA was stained with DAPI (right). mNeonGreen and DAPI signals colocalized very well and individual virions are easily distinguishable. Approximately 1.4% of the fluorescent phage particles examined (6 out of 438) lacked the mNeonGreen signal. **b**, Overlay images (phase contrast and fluorescent channels) from a time-lapse video depicting a representative PAO1 cell being infected by a *gp93-mNeonGreen* mutant phage. *gp93-mNeonGreen* and phage DNA are shown as green and blue signals, respectively. The representative cell was chosen out of 1,093 infected cells from two independent infection experiments. **c**, Overlay images from a time-lapse video showing a PAO1 cell being infected by a WT ΦKZ loaded with gp93-mNeonGreen fusion proteins. The representative cell was chosen out of 1,045 infected cells from two independent infection experiments. gp93-mNG, gp93-mNeonGreen. Scale bar, 2 μm.

activities against different *orf11*-targeting crRNAs, indicating that the incorporated *acrVIA1* was expressed and properly functioning (Fig. 5c). No other significant change in plaque size or efficiency was observed for the PaMx41 *orf24::acrVIA1* phage on strain PAO1. This mutant displayed decreased plaquing ability in another *P. aeruginosa* strain; however, this has now been more thoroughly characterized in a separate publication[41]. Notably, initial PCR screening for recombinant plaques showed that 100% of surviving phages were desired recombinants, with no spontaneous escape plaques. The data suggest that the RNA-targeting Cas13a system holds great promise for becoming a universal genetic editing tool to deal with previously intractable phages.

Conclusions

We applied the RNA-targeting CRISPR–Cas13a system, in conjunction with homologous recombination, to achieve genetic modification of the jumbo phages ΦKZ and OMKO1, and the small podophage PaMx41, all of which are resistant to DNA-targeting CRISPR–Cas systems. CRISPR–Cas13a-mediated counterselection recovered rare (approximately 10^{-5}) phage recombinants from a large pool of WT phages. It is notable that despite the phage nucleus present in jumbo phage ΦKZ, which renders the ΦKZ genome inaccessible to many bacterial proteins, the editing plasmid DNA can interact with the ΦKZ genome to recombine with expected frequencies.

Many studies reported that phages can hamper CRISPR–Cas activities, for example, by repressing transcription of endogenous CRISPR–Cas components[42,43], possessing covalent DNA modifications[44–47] or encoding anti-CRISPR proteins (recently reviewed in Davidson et al.[48]). Furthermore, the assembly of a proteinaceous nucleus-like structure that shields phage genomes from attack by distinct DNA-targeting nucleases[20,21] represents the ultimate 'anti-CRISPR/anti-restriction modification' mechanism. Therefore, development of phage genomic manipulation approaches that target mRNA, which is a relatively consistent and exposed molecule, may provide a near-universal approach. Moreover, Cas13 is rarely encoded in bacteria[49,50] and most phages are therefore not expected to encode anti-Cas13a proteins.

Applying gene editing to ΦKZ allowed us to query endogenous gene function and essentiality for the first time. We observed that Δ*phuZ* mutant phages mispositioned the phage nucleus during viral intracellular development. Previous studies revealed that newly assembled phage capsids trafficked along the PhuZ filaments towards the phage nucleus for viral DNA packaging[32]. However, our work demonstrates that successful DNA loading into capsids is not dependent on

https://doi.org/10.1038/s41564-022-01243-4

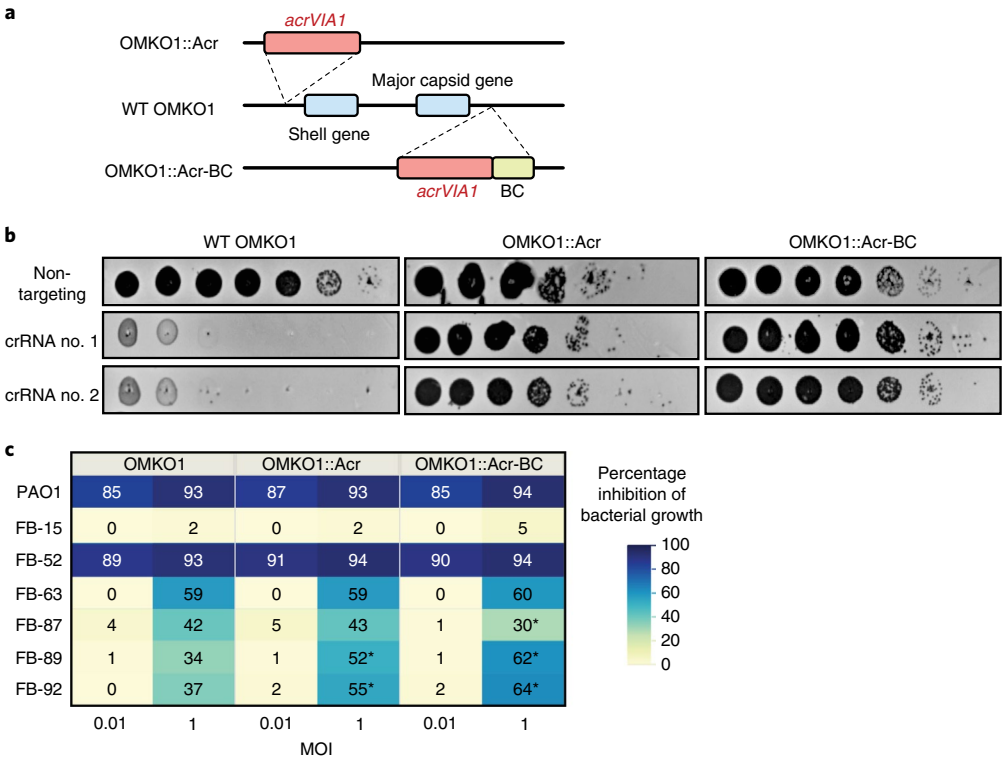

Fig. 4 | Genetic engineering of the therapeutic jumbo phage OMKO1. **a**, Schematic of genomes of two engineered OMKO1 variants where the indicated gene fragments were integrated into the WT genome. OMKO1::Acr: *acrVIA1* was inserted upstream of the shell gene. OMKO1::Acr-BC: *acrVIA1* was inserted together with a barcode sequence (BC) downstream of the major capsid gene. **b**, Plaque assays of WT OMKO1 and mutants on lawns expressing *cas13* and crRNAs targeting the OMKO1 homologues of the ΦKZ *orf120* (crRNA no. 1) or *orf146* (crRNA no. 2) transcripts. **c**, Determination of the host range of WT OMKO1 and mutants on representative *P. aeruginosa* clinical strains by microplate liquid assay at MOI of 0.01 and 1. Data are presented as the mean liquid assay scores across three independent experiments. The asterisk indicates a significant difference between WT and mutants as determined by a two-sided Student's *t*-test ($P < 0.05$). The colour intensity of each phage-host combination reflects the liquid assay score; the darker the colour the stronger the intensity displaying a greater score. The liquid assay score represents how well the phage strain can repress the growth of a given bacterial host. No inhibition of bacterial growth is reflected by a liquid assay score of 0, while complete suppression would result in a score of 100. (The full table of plaque assays is shown in Extended Data Fig. 6).

PhuZ. Moreover, loss of PhuZ appeared to lower burst size, but did not impact host range or plaque morphology. Overall, *phuZ* seems to be a bona fide non-essential gene for ΦKZ. The evolutionary advantage of encoding tubulin in this jumbo phage and many others requires further investigation. Furthermore, a fluorescent label on gp93 demonstrated that it is packaged in the phage head, injected with the genome and massively synthesized later during infection, with peri-nuclear localization. The labelling not only allows us to visualize individual virions under the microscope but also to observe the injection of this inner body protein into the host cell, which had been previously suggested with little evidence[36,51].

One major challenge of using Cas13a, in our experience, has been the wide variability of crRNA efficacy. Future studies focusing on the optimization of crRNA design for phage targeting or perhaps the implementation of other RNA-targeting enzymes, such as Cas13 orthologues or Cas7-11 (refs. [52,53]) will be important. However, we can circumvent this problem by implementing an anti-CRISPR selectable marker[17] to ensure that the same strong guide can be used for all genetic manipulations for a given phage strain. The downside is that this limits the user to a single perturbation and leaves the *acr* gene in the phage genome. However, double and triple mutants are possible in principle if one uses crRNAs specific to the site of editing[50], negating the need for an *acr* gene. One could also remove the *acr* gene from the genome, for example, with the introduction of flippase (FLP) recombination sites and a phage nucleus-localized FLP recombinase.

In summary, the RNA-targeting CRISPR–Cas13a counterselection tool should be applicable to a broad range of phages and enable downstream high throughput phage engineering. In addition to the double-stranded DNA (dsDNA) phage efficacy demonstrated in this study, this approach could also be suitable, in principle, to engineer single-stranded DNA phages. The ability to generate synthetic phages precisely and efficiently with desired features will not only benefit phage therapeutic applications but will also advance our understanding of fundamental phage biology and phage-bacteria interactions.

Methods

Strains, DNA oligonucleotides and plasmid constructions

All bacterial and phage strains, plasmids, spacer sequences, and primers used in this study are listed in Supplementary Tables 1–4, respectively.

The crRNAs designed for CRISPR–Cas13 targeting were constructed in the pHERD30T backbone. The pHERD30T-crRNA V2 was constructed by thermal annealing of the oligonucleotides oSDM465 and oSDM466 and phosphorylation by polynucleotide kinase. The annealed product was introduced by Gibson assembly into pHERD30T linearized by PCR using the oligonucleotides oSDM457 and oSDM458. Proper construction of the expression vector was verified by Sanger sequencing. The pHERD30T-crRNA V3 was constructed just as for V2, but the crRNA-coding insert was instead composed of the oligonucleotides oSDM455 and oSDM456. Both V2 and V3 of this plasmid were designed such that cleavage by BsaI would generate a linear plasmid that would accept annealed oligonucleotide spacers via ligation. Oligonucleotide pairs with repeat-specific overhangs encoding spacer sequences were annealed and phosphorylated using T4 polynucleotide

https://doi.org/10.1038/s41564-022-01243-4

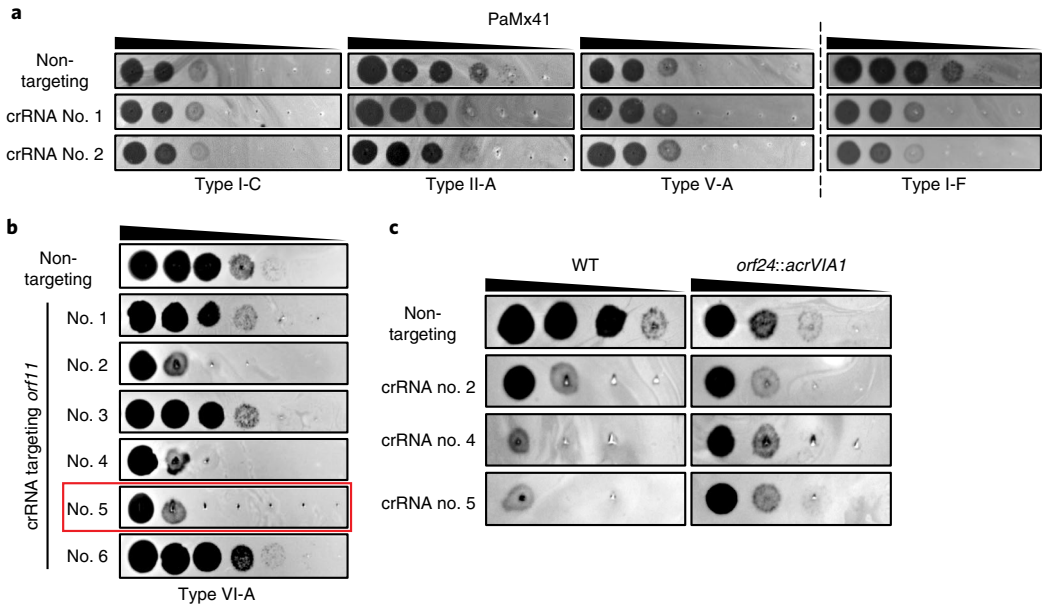

Fig. 5 | Genetic engineering of podophage PaMx41. a, Plaque assays with ten-fold serial dilutions of PaMx41 plated on lawns expressing the indicated CRISPR-Cas subtype together with two different crRNA sequences each, or **b**, while being targeted by CRISPR–Cas13a. The crRNA sequences of different CRISPR–Cas systems are listed in Supplementary Table 3. crRNA no. 5 highlighted in the red frame was used for PaMx41 genome engineering. **c**, Engineered variants of PaMx41 *orf24::acrVIA1* plated in ten-fold serial dilutions on lawns expressing *cas13* and different crRNA sequences.

kinase and then cloned into the BsaI-digested empty vectors. Cloning procedures were performed in commercial *Escherichia coli* DH5α cells (New England Biolabs) according to the manufacturer's protocols. The resulting crRNA plasmids were electroporated into the *P. aeruginosa* PAO1 strain harbouring the *tn7::cas13a*^{Lse} (SDM084) on the chromosome as described previously[20]. Gene expression was induced by the addition of L-arabinose at a final concentration of 0.3% and isopropyl-β-D-thiogalactopyranoside (IPTG) at a final concentration of 1 mM.

To construct editing plasmids for homologous recombination, homology arms of >500 bp in length were amplified by PCR using the ΦKZ genomic DNA as the template. To prevent Cas13a cleavage, several synonymous mutations were introduced into the crRNA-targeting site of the left *orf120* homology arm by designing the reverse primer (JG064) to contain appropriate mismatches. The *acrVIA1* gene was amplified from the plasmid pAM383 (ref. [25]), a gift from L. Marraffini (The Rockefeller University). PCR products were purified and assembled as a recombineering substrate and then inserted into the NheI site of the pHERD30T backbone by Gibson assembly (New England Biolabs) according to the manufacturer's protocols. The resulting plasmids were electroporated into PAO1.

To construct plasmids to complement WT PhuZ, gp54 and gp146 of ΦKZ *in trans*, *phuZ*, *orf54* or operon no. 24 (containing both *orf53* and *orf54*), or *orf146* were amplified by PCR using the ΦKZ genomic DNA as the template. The PCR products were then cloned into the pHERD30T backbone at either the NheI recognition site or between two different restriction sites. The resulting plasmids were introduced into PAO1 by electroporation. Thereafter, mutant phages were used to infect the appropriate PAO1 strains carrying the corresponding plasmid for complementation.

Isolation of phage recombinants

Host strains bearing editing plasmids were grown in lysogeny broth (LB) supplemented with 10 mM $MgSO_4$ and 50 μg ml^{-1} gentamicin, at 37 °C with aeration at 250 r.p.m. When OD_{600} was around 2, WT ΦKZ was added into the culture at an MOI of 1 to allow infection to occur for approximately 18 h; 2% volume of chloroform was added into the infection culture and left to shake gently on an orbital shaker at room temperature for 15 min, followed by centrifugation at 4,000*g* for 15 min to remove cell debris. The supernatant lysate was further treated with 2% chloroform for 15 min and centrifuged again under the same conditions, followed by a 30-min treatment with DNase I (New England Biolabs) at 37 °C. The resulting phage lysate containing both WT phages and recombinants were titrated on PAO1 strains bearing the CRISPR–Cas13a system with the most efficient crRNA (*orf120* crRNA no. 2) to screen for recombinants. Individual phage plaques were picked from top agar and purified for three rounds using the CRISPR counterselection strain to ensure thorough removal of any remaining WT phages. Whether or not they were recombinant phages or Cas13a escape phages was determined by PCR using appropriate pairs of primers amplifying the modified regions of the phage genome. Identified phages were further confirmed and analysed by sequencing the PCR products or the whole genomes and then stored at 4 °C.

Phage plaque assay

Host strains were grown in LBM (LB supplemented with 10 mM $MgSO_4$), 50 μg ml^{-1} gentamicin, 1 mM IPTG and 0.3% arabinose inducers for gene expression, at 37 °C with aeration at 250 r.p.m. overnight. Phage spotting assays were performed using 1.5% LB agar plates and 0.42% LB top agar, both of which contained 10 mM $MgSO_4$ and inducers. Then, 100 μl of appropriate overnight culture was suspended in 3.5 ml of molten top agar and poured onto an LB + 10 mM $MgSO_4$ agar plate, leading to the growth of a bacterial lawn. After 10–15 min at room temperature, 2 μl of tenfold serial dilutions of phages was spotted onto the solidified top agar. Plates were incubated overnight at 37 °C. Plate images were obtained using the Gel Doc EZ Gel Documentation System (Bio-Rad Laboratories) and Image Lab v.6.0.1 (Bio-Rad Laboratories).

Microplate liquid assay

Fresh overnight cultures were diluted to a cell concentration of 1×10^8 colony-forming units per ml in LB medium supplemented with 10 mM $MgSO_4$. Phage lysates were added to reach an MOI of approximately 1 and 0.01 in a Corning Costar 96-well clear flat-bottom microplate (Thermo Fisher Scientific) sealed with a Breathe-Easy sealing

membrane (Merck). After the infection cultures were incubated at room temperature for 20 min, plates were incubated at 37 °C, 800 r.p.m. for 8 h in a BioTek LogPhase 600 plate reader (Agilent Technologies). Cell growth was monitored by measuring OD_{600} every 20 min. Each phage-host combination was performed in three biological replicates.

Data analysis

Growth curves for each phage-host combination were obtained by plotting OD_{600} after blank correction (baseline adjustment) against time. Each growth curve was transformed into a single numerical value by calculating the area under the curve (AUC) using the trapezoid method. Then, AUCs were normalized as a percentage of the AUC of their corresponding uninfected control according to the following equation:

$$\text{Liquid assay score} = \frac{\text{AUC(positive control)} - \text{AUC(phage treatment)}}{\text{AUC(positive control)}} \times 100$$

The resulting value, defined as the 'liquid assay score', represents how well the phage strain can repress the growth of a bacterial population over the course of the 8-h experiment. No inhibition of bacterial growth would result in a liquid assay score of 0 and complete suppression would translate into a score of 100. Liquid assay scores were averaged using data from three biological replicates.

One-step growth curve

Phage burst size was determined by one-step growth curve experiments. The host PAO1 strain was grown in LBM medium to an OD_{600} of approximately 0.4 at 37 °C with aeration at 250 r.p.m. Then, 1 ml of the cell culture was mixed with the phage lysate to achieve an MOI of 0.01. The mixture was incubated in a 37 °C heat block for 10 min for infection. Then, 100 µl of the infection mixture was added to 4.9 ml of fresh, pre-warmed LBM and incubated at 37 °C with shaking at 250 r.p.m. The initial phage titre was determined by phage titration. At 1 min from this point, 950 µl of the culture was transferred into an Eppendorf tube supplied with 50 µl chloroform, followed by phage titration to calculate the number of free phages. Samples were collected at 15-min or 10-min intervals for approximately 120 min and phage titres were determined immediately. Phage titres at different time points were plotted against time to determine the latent period and burst size of each phage strain. Phage burst sizes were calculated by dividing the average phage titres at the plateau phase by the initial phage titres after subtracting free phages. Assays were performed at least as three biological replicates for each phage strain and burst sizes are the mean of three or four measurements.

Single-cell infection assay

A single colony was inoculated in 1 ml of LBM supplied with 50 µg ml^{-1} gentamicin (if necessary) and grown at 37 °C with 250 r.p.m. shaking overnight. The overnight culture was diluted 100-fold in 5 ml of LBM and grown at 37 °C with 250 r.p.m. shaking to an OD_{600} of approximately 0.4. Next, 1 ml of the cell culture was collected by centrifugation at 3,000*g* for 2 min at room temperature and concentrated by 25-fold in fresh LBM. Then, 10 µl of cells were mixed with 10 µl of appropriate phage strains to reach an appropriate MOI, followed by incubation at 30 °C for 10 min to allow for phage infection. The infection mixture was further diluted by tenfold into 50 µl of fresh LBM at room temperature; 1 µl of the diluted culture was gently placed onto a piece of agarose pad (approximately 1 mm thick) with 1:5 diluted LBM, arabinose (0.8%) and 4′,6-diamidino-2-phenylindole (DAPI) (5 µg ml^{-1}; no.153, catalogue no. D1306; Invitrogen). A coverslip (no. 1.5; Thermo Fisher Scientific) was gently laid over the agarose pad and the sample was imaged under a fluorescence microscope at 30 °C within a cage incubator to maintain temperature and humidity.

Fluorescence microscopy and imaging

Microscopy was performed on an inverted epifluorescence microscope (Ti2-E; Nikon) equipped with the Perfect Focus System and a Photometrics Prime 95B 25-mm camera. Image acquisition and processing were performed with the Nikon Elements AR software v.5.02.00 (64-bit). During a time-lapse video, the specimen was typically imaged at a time interval of 5 min at the focal plane for 2.5–3 h, through channels of phase contrast (200 ms exposure for cell recognition), blue (DAPI, 200 ms exposure for phage DNA) and green (green fluorescent protein, 300 ms exposure for gp93-mNeonGreen).

Next-generation sequencing

To isolate phage genomic DNA, purified high titre lysates were treated with benzonase nuclease (Sigma-Aldrich) for 30 min at 37 °C. Phage genomic DNA was extracted according to a modified Wizard DNA Clean-Up Kit (Promega Corporation) protocol. To bind DNA to the column, we kept a ratio of 1:2 lysate:Wizard DNA Clean-Up resin. In the elution step,100 µl of pre-warmed H_2O was added to the column and immediately centrifuged at 13,000*g* for 1 min to elute DNA. DNA samples were quantified with the AccuGreen Broad Range dsDNA quantification kit (Biotium) in a Qubit Fluorometer 2.0.

Purified phage genomic DNA was processed according to the Illumina DNA preparation protocol. Samples were sequenced on a MiSeq system (Illumina) with 300 cycles of paired-end sequencing and loading concentration of 12 pM. Illumina short reads were downsampled to approximately 50–100× coverage and de novo assembled using SPAdes 3.14.1. The sequences of mutant phage strains were aligned to the reference genome in Geneious Prime® 2021.2.2 with the Mauve alignment algorithm to confirm the intended genomic edits.

The isolated *orf54* 'pseudo knockout' phage strain (Δ*orf54*) was sequenced using long-read sequencing. DNA samples were processed using the SQK-LSK109 kit (Oxford Nanopore Technologies). Libraries were sequenced using an R10.3 flow cell until the desired number of reads was achieved. Oxford Nanopore long reads were filtered for the longest high-quality reads using NanoFilt v2.6.0 and de novo assembled using Flye 2.8.2.

Reporting summary

Further information on research design is available in the Nature Research Reporting Summary linked to this article.

Data availability

All relevant data are included in the paper and/or its supplementary information files. The complete genome sequence of OMKO1 was deposited in GenBank under accession no. ON631220. All strains and plasmids are available from the corresponding author upon reasonable request. Source data are provided with this paper.

Code availability

The data analysis code is available from public repositories at https://zenodo.org/record/6324407#.YiAjrejMI2w.

References

1. Kortright, K. E., Chan, B. K., Koff, J. L. & Turner, P. E. Phage therapy: a renewed approach to combat antibiotic-resistant bacteria. *Cell Host Microbe* **25**, 219–232 (2019).
2. Pires, D. P., Cleto, S., Sillankorva, S., Azeredo, J. & Lu, T. K. Genetically engineered phages: a review of advances over the last decade. *Microbiol. Mol. Biol. Rev.* **80**, 523–543 (2016).
3. Doss, J., Culbertson, K., Hahn, D., Camacho, J. & Barekzi, N. A review of phage therapy against bacterial pathogens of aquatic and terrestrial organisms.*Viruses* **9**, 50 (2017).
4. Nobrega, F. L., Costa, A. R., Kluskens, L. D. & Azeredo, J. Revisiting phage therapy: new applications for old resources. *Trends Microbiol.* **23**, 185–191 (2015).

5. Łusiak-Szelachowska, M. et al. Phage neutralization by sera of patients receiving phage therapy. *Viral Immunol.* **27**, 295–304 (2014).
6. Weber-Dąbrowska, B. et al. Bacteriophage procurement for therapeutic purposes. *Front. Microbiol.* **7**, 1177 (2016).
7. Lu, T. K. & Koeris, M. S. The next generation of bacteriophage therapy. *Curr. Opin. Microbiol.* **14**, 524–531 (2011).
8. Lenneman, B. R., Fernbach, J., Loessner, M. J., Lu, T. K. & Kilcher, S. Enhancing phage therapy through synthetic biology and genome engineering. *Curr. Opin. Biotechnol.* **68**, 151–159 (2021).
9. Ando, H., Lemire, S., Pires, D. P. & Lu, T. K. Engineering modular viral scaffolds for targeted bacterial population editing. *Cell Syst.* **1**, 187–196 (2015).
10. Mahichi, F., Synnott, A. J., Yamamichi, K., Osada, T. & Tanji, Y. Site-specific recombination of T2 phage using IP008 long tail fiber genes provides a targeted method for expanding host range while retaining lytic activity. *FEMS Microbiol. Lett.* **295**, 211–217 (2009).
11. Matsuda, T. et al. Lysis-deficient bacteriophage therapy decreases endotoxin and inflammatory mediator release and improves survival in a murine peritonitis model. *Surgery* **137**, 639–646 (2005).
12. Monteiro, R., Pires, D. P., Costa, A. R. & Azeredo, J. Phage therapy: going temperate? *Trends Microbiol.* **27**, 368–378 (2019).
13. Kilcher, S. & Loessner, M. J. Engineering bacteriophages as versatile biologics. *Trends Microbiol.* **27**, 355–367 (2019).
14. Marinelli, L. J., Hatfull, G. F. & Piuri, M. Recombineering: a powerful tool for modification of bacteriophage genomes. *Bacteriophage* **2**, 5–14 (2012).
15. Deveau, H., Garneau, J. E. & Moineau, S. CRISPR/Cas system and its role in phage-bacteria interactions. *Annu. Rev. Microbiol.* **64**, 475–493 (2010).
16. Hille, F. et al. The Biology of CRISPR–Cas: backward and forward. *Cell* **172**, 1239–1259 (2018).
17. Mayo-Muñoz, D. et al. Anti-CRISPR-based and CRISPR-based genome editing of *Sulfolobus islandicus* rod-shaped virus 2.*Viruses* **10**, 695 (2018).
18. Samson, J. E., Magadan, A. H., Sabri, M. & Moineau, S. Revenge of the phages: defeating bacterial defences. *Nat. Rev. Microbiol.* **11**, 675–687 (2013).
19. Malone, L. M., Birkholz, N. & Fineran, P. C. Conquering CRISPR: how phages overcome bacterial adaptive immunity. *Curr. Opin. Biotechnol.* **68**, 30–36 (2021).
20. Mendoza, S. D. et al. A bacteriophage nucleus-like compartment shields DNA from CRISPR nucleases. *Nature* **577**, 244–248 (2020).
21. Malone, L. M. et al. A jumbo phage that forms a nucleus-like structure evades CRISPR–Cas DNA targeting but is vulnerable to type III RNA-based immunity. *Nat. Microbiol.* **5**, 48–55 (2020).
22. Guan, J. & Bondy-Denomy, J.Intracellular organization by jumbo bacteriophages.*J. Bacteriol.* **203**, e00362-20 (2020).
23. Abudayyeh, O. O. et al. C2c2 is a single-component programmable RNA-guided RNA-targeting CRISPR effector. *Science* **353**, aaf5573 (2016).
24. Meeske, A. J., Nakandakari-Higa, S. & Marraffini, L. A. Cas13-induced cellular dormancy prevents the rise of CRISPR-resistant bacteriophage. *Nature* **570**, 241–245 (2019).
25. Meeske, A. J. et al. A phage-encoded anti-CRISPR enables complete evasion of type VI-A CRISPR–Cas immunity. *Science* **369**, 54–59 (2020).
26. East-Seletsky, A. et al. Two distinct RNase activities of CRISPR–C2c2 enable guide-RNA processing and RNA detection. *Nature* **538**, 270–273 (2016).
27. Meeske, A. J. & Marraffini, L. A. RNA guide complementarity prevents self-targeting in type VI CRISPR systems. *Mol. Cell* **71**, 791–801.e3 (2018).
28. M Iyer, L., Anantharaman, V., Krishnan, A., Maxwell Burroughs, A. & Aravind, L. Jumbo phages: a comparative genomic overview of core functions and adaptions for biological conflicts.*Viruses* **13**, 63 (2021).
29. Al-Shayeb, B. et al. Clades of huge phages from across Earth's ecosystems. *Nature* **578**, 425–431 (2020).
30. Aylett, C. H. S., Izoré, T., Amos, L. A. & Löwe, J. Structure of the tubulin/FtsZ-like protein TubZ from *Pseudomonas* bacteriophage ΦKZ. *J. Mol. Biol.* **425**, 2164–2173 (2013).
31. Chaikeeratisak, V. et al. The phage nucleus and tubulin spindle are conserved among large *Pseudomonas* phages. *Cell Rep.* **20**, 1563–1571 (2017).
32. Chaikeeratisak, V. et al. Viral capsid trafficking along treadmilling tubulin filaments in bacteria. *Cell* **177**, 1771–1780.e12 (2019).
33. Kraemer, J. A. et al. A phage tubulin assembles dynamic filaments by an atypical mechanism to center viral DNA within the host cell. *Cell* **149**, 1488–1499 (2012).
34. Chaikeeratisak, V. et al. Assembly of a nucleus-like structure during viral replication in bacteria. *Science* **355**, 194–197 (2017).
35. Wu, W., Thomas, J. A., Cheng, N., Black, L. W. & Steven, A. C. Bubblegrams reveal the inner body of bacteriophage ΦKZ. *Science* **335**, 182 (2012).
36. Thomas, J. A. et al. Extensive proteolysis of head and inner body proteins by a morphogenetic protease in the giant *Pseudomonas aeruginosa* phage ΦKZ. *Mol. Microbiol.* **84**, 324–339 (2012).
37. Chan, B. K. et al. Phage selection restores antibiotic sensitivity in MDR *Pseudomonas aeruginosa*. *Sci. Rep.* **6**, 26717 (2016).
38. Chan, B. K. et al. Phage treatment of an aortic graft infected with *Pseudomonas aeruginosa*. *Evol. Med. Public Health* **2018**, 60–66 (2018).
39. Sepúlveda-Robles, O., Kameyama, L. & Guarneros, G. High diversity and novel species of *Pseudomonas aeruginosa* bacteriophages. *Appl. Environ. Microbiol.* **78**, 4510–4515 (2012).
40. Cruz-Plancarte, I., Cazares, A. & Guarneros, G. Genomic and transcriptional mapping of PaMx41, archetype of a new lineage of bacteriophages infecting *Pseudomonas aeruginosa*. *Appl. Environ. Microbiol.* **82**, 6541–6547 (2016).
41. Huiting, E. et al. Bacteriophages antagonize cGAS-like immunity in bacteria. Preprint at *bioRxiv* https://doi.org/10.1101/2022.03.30.486325 (2022).
42. Skennerton, C. T. et al. Phage encoded H-NS: a potential Achilles heel in the bacterial defence system. *PLoS ONE* **6**, e20095 (2011).
43. Pul, U. et al. Identification and characterization of *E. coli* CRISPR–*cas* promoters and their silencing by H-NS. *Mol. Microbiol.* **75**, 1495–1512 (2010).
44. Hampton, H. G., Watson, B. N. J. & Fineran, P. C. The arms race between bacteria and their phage foes. *Nature* **577**, 327–336 (2020).
45. Vlot, M. et al. Bacteriophage DNA glucosylation impairs target DNA binding by type I and II but not by type V CRISPR–Cas effector complexes. *Nucleic Acids Res.* **46**, 873–885 (2018).
46. Bryson, A. L. et al. Covalent modification of bacteriophage T4 DNA inhibits CRISPR–Cas9. *mBio* **6**, e00648 (2015).
47. Liu, Y. et al. Covalent modifications of the bacteriophage genome confer a degree of resistance to bacterial CRISPR systems.*J. Virol.* **94**, e01630-20 (2020).
48. Davidson, A. R. et al. Anti-CRISPRs: protein inhibitors of CRISPR–Cas systems. *Annu. Rev. Biochem.* **89**, 309–332 (2020).
49. Makarova, K. S. et al. Evolutionary classification of CRISPR–Cas systems: a burst of class 2 and derived variants. *Nat. Rev. Microbiol.* **18**, 67–83 (2020).
50. Adler, B. et al. RNA-targeting CRISPR–Cas13 provides broad-spectrum phage immunity. Preprint at *bioRxiv* https://doi.org/10.1101/2022.03.25.485874 (2022).

51. Krylov, V. N. et al. *Pseudomonas* bacteriophage ΦKZ contains an inner body in its capsid. *Can. J. Microbiol.* **30**, 758–762 (1984).
52. van Beljouw, S. P. B. et al. The gRAMP CRISPR–Cas effector is an RNA endonuclease complexed with a caspase-like peptidase. *Science* **373**, 1349–1353 (2021).
53. Özcan, A. et al. Programmable RNA targeting with the single-protein CRISPR effector Cas7-11. *Nature* **597**, 720–725 (2021).

Acknowledgements

The Bondy-Denomy lab was supported by the National Institutes of Health (no. R01GM127489 and R01AI171041), Vallee Foundation, Searle Scholarship, Innovative Genomics Institute and University of California San Francisco Program for Breakthrough Biomedical Research funded in part by the Sandler Foundation. This work was also supported by research funds from Felix Biotechnology. We thank L. Marraffini (The Rockefeller University) for providing the plasmid pAM383. We thank P. Turner and B. Chan (Yale University) for providing the OMKO1 phage and *P. aeruginosa* clinical isolates. We thank G. Guarneros Peña at Centro de Investigación y de Estudios Avanzados for providing the PaMx41 phage. We thank T. Rotstein for his generous assistance with NGS data processing and interpretation. We thank members of the Bondy-Denomy laboratory for productive conversations and generous suggestions for our work.

Author contributions

J.G. designed and performed the experiments, analysed the data and wrote the manuscript. A.O.-B. performed phage plaque and microplate liquid assays and analysed the data. S.D.M. designed and constructed the Cas13a crRNA vectors. S.K. conducted the phage plaque assays for phage PaMx41. J.B. performed NGS and analysed the data. J.B.-D. conceived and supervised the study, designed the experiments, acquired the funding and wrote the manuscript.

Competing interests

J.B.-D. is a scientific advisory board member of SNIPR BIOME, Excision BioTherapeutics and Leapfrog Bio, and a scientific advisory board member and cofounder of Acrigen Biosciences. The Bondy-Denomy laboratory receives research support from Felix Biotechnology. The other authors declare no competing interests.

Additional information

Extended data is available for this paper at https://doi.org/10.1038/s41564-022-01243-4.

Supplementary information The online version contains supplementary material available at https://doi.org/10.1038/s41564-022-01243-4.

Correspondence and requests for materials should be addressed to Joseph Bondy-Denomy.

Peer review information *Nature Microbiology* thanks Anne Chevallereau and the other, anonymous, reviewer(s) for their contribution to the peer review of this work.

Reprints and permissions information is available at www.nature.com/reprints.

Publisher's note Springer Nature remains neutral with regard to jurisdictional claims in published maps and institutional affiliations.

https://doi.org/10.1038/s41564-022-01243-4

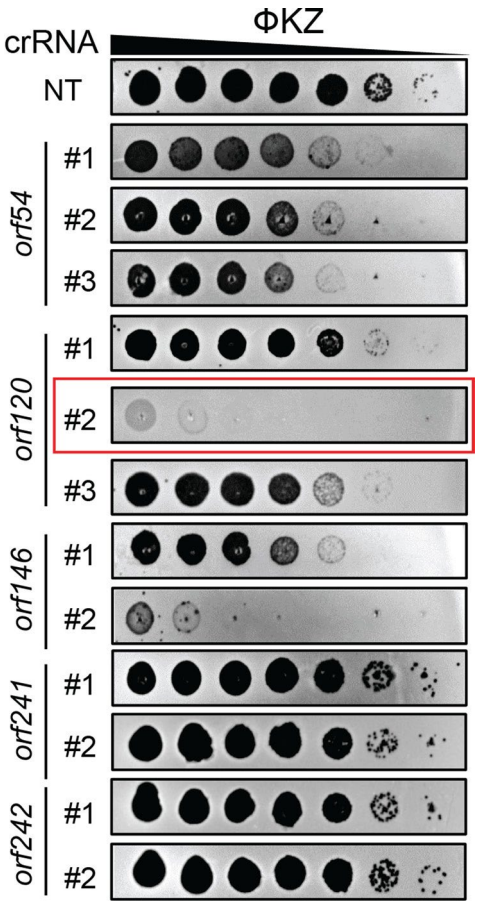

Extended Data Fig. 1 | Plaque efficiency assays of distinct crRNAs of CRISPR-Cas13a targeting transcripts of diverse ΦKZ genes. Ten-fold serial dilutions of ΦKZ spotted on lawns expressing *cas13* and crRNAs targeting the indicated genes. The crRNA targeting orf120 highlighted in the red frame has been used for ΦKZ genome engineering. NT, non-targeting.

https://doi.org/10.1038/s41564-022-01243-4

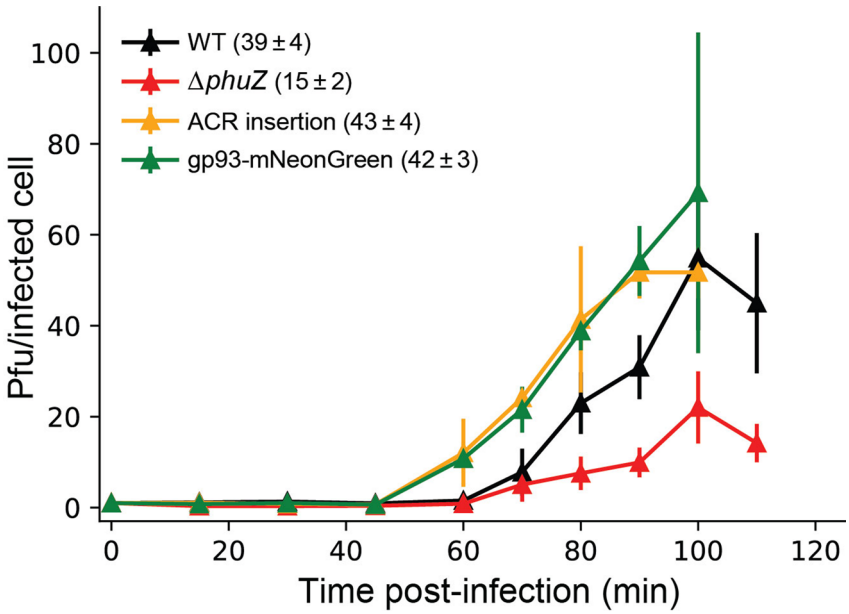

Extended Data Fig. 2 | One-step growth curves of engineered ΦKZ variants. One-step growth curve experiment was performed to determine the latent time period and burst size of engineered phages. Representative plots are shown for each phage strain. The burst sizes are shown in brackets after of each ΦKZ variant, representing the mean ± standard error of three or four biologically independent replicates.

https://doi.org/10.1038/s41564-022-01243-4

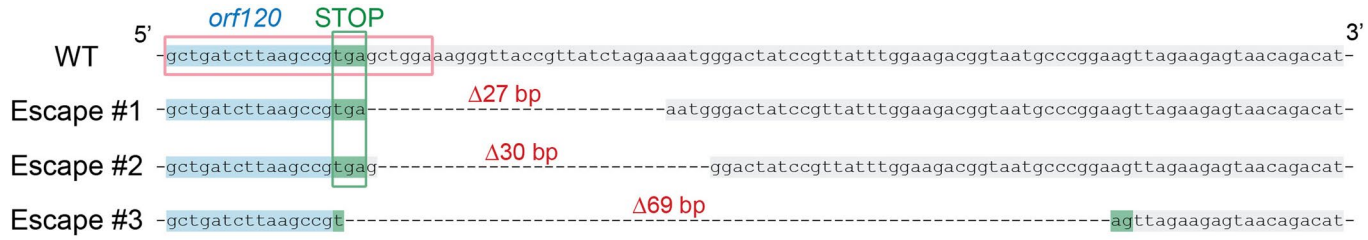

Extended Data Fig. 3 | Sequence alignment of wild type ΦKZ and three escape mutants at the engineered genomic site. Escape mutants were isolated and verified by PCR and sequencing. The WT *orf120* sequence is highlighted in blue and the downstream region is highlighted in grey. The stop codon (TGA) of *orf120* is highlighted in green and Escape mutant #3 reconstitutes it to TAG. The sequence in the red frame matches the spacer sequence of the crRNA that was used to target and eliminate WT phages. Deletions were indicated by dashed lines and their corresponding numbers of absent base pairs.

https://doi.org/10.1038/s41564-022-01243-4

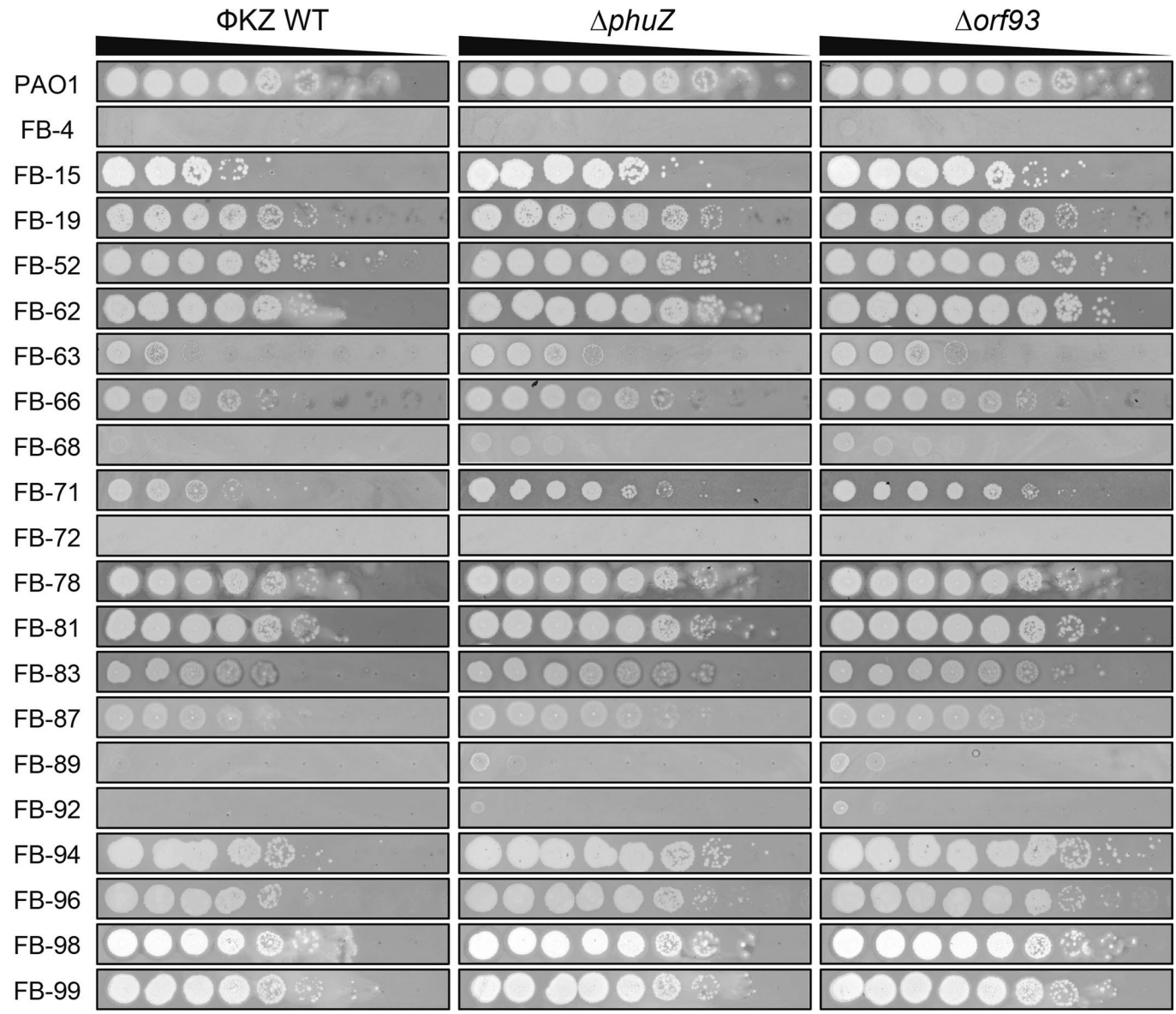

Extended Data Fig. 4 | Determination of host range of ΦKZ Δ*phuZ* and Δ*orf93* mutants by plaque assay on *P. aeruginosa* clinical strains. Spot-titration of the indicated ΦKZ phages on lawns of clinical isolates of *P. aeruginosa* (FB-XX).

https://doi.org/10.1038/s41564-022-01243-4

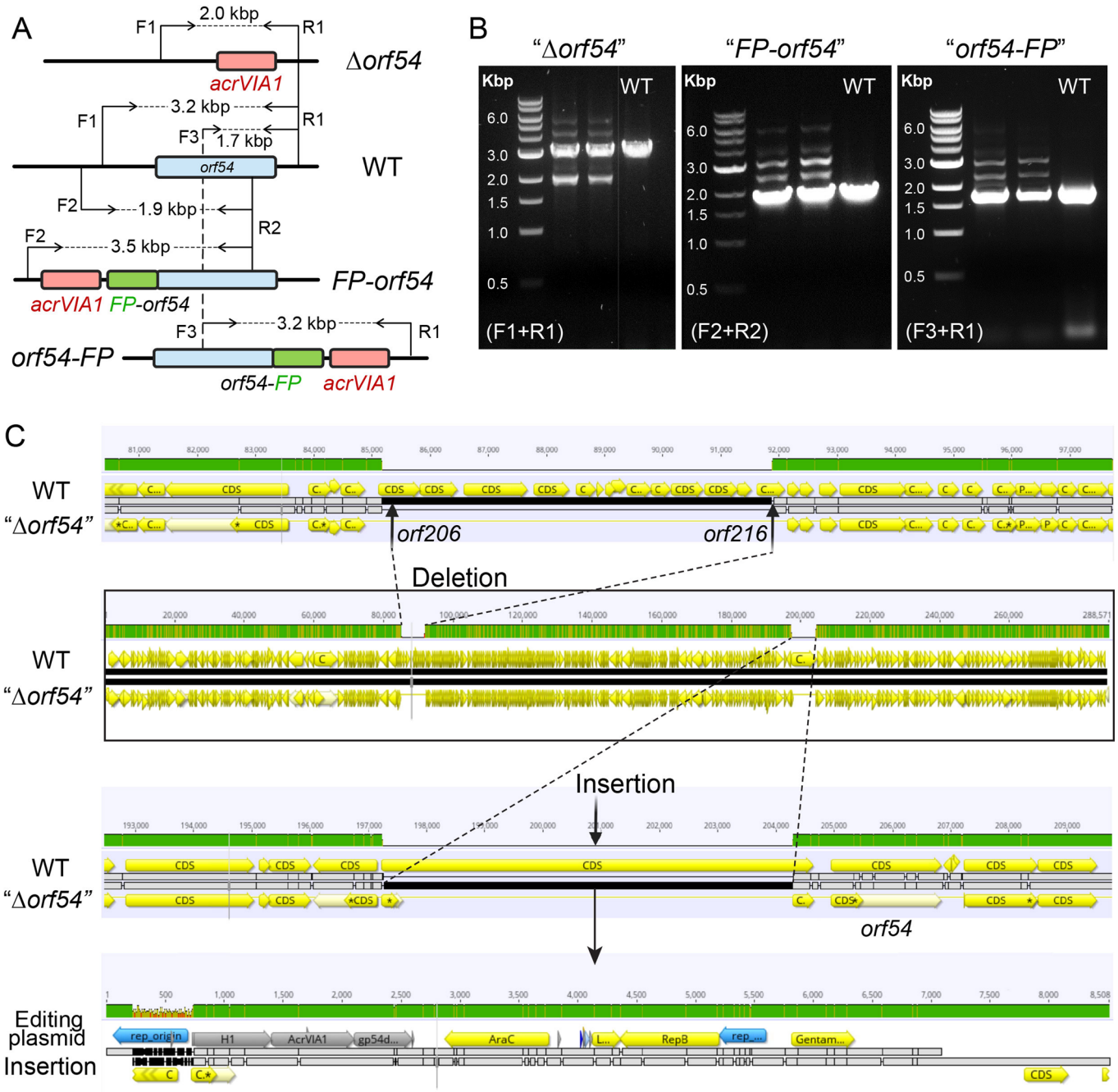

Extended Data Fig. 5 | Failure of genetic editing the shell gene (*orf54*) in ΦKZ. (A) Schematic of genomes of WT ΦKZ and three mutated *orf54* variants, "Δ*orf54*", "*FP-orf54*", and "*orf54-FP*", at the editing site. *orf54*, *acrVIA1*, and fluorescent protein (FP) are shown as blue, red, and green rectangles, respectively. F and R indicate forward and reverse primers, respectively, for PCR confirmation of *orf54* engineering. (B) PCR confirmation of the indicated *orf54* mutants using their corresponding pair of primers. All three mutants generated multiple bands, including a band in the same size as the single band produced by WT. PCR-based screening for engineered ΦKZ *orf54* variants have been independently repeated at least three times yielding similar results. (C) Genome alignment of WT phage with the isolated *orf54* "*pseudo* knock-out" mutant ("Δ*orf54*"). A gene cluster of ~ 7 kbp (*orf206* - *orf216*) was missing in the mutant, likely as a result of phage packaging capacity. The majority of the editing plasmid used to generate recombinants was at the editing site, leaving *orf54* intact.

https://doi.org/10.1038/s41564-022-01243-4

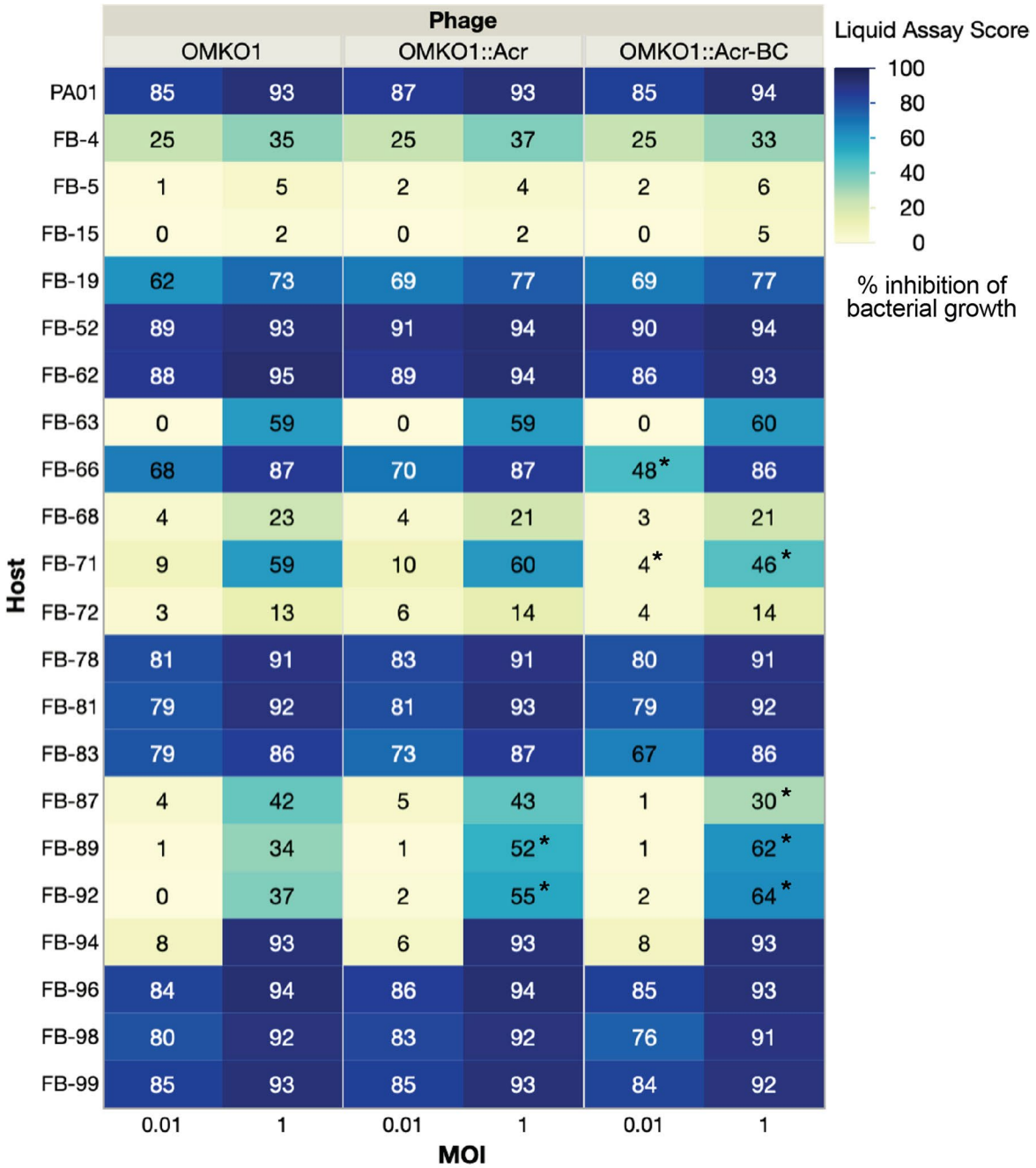

Extended Data Fig. 6 | Host range assay of engineered OMKO1 variants. Host ranges were determined by microplate liquid assay at MOI of 0.01 and 1 on 22 *P. aeruginosa* clinical strains. The values are presented as the mean liquid assay scores across three independent experiments. Asterisks (*) indicate significant difference between WT and engineered strains as determined by two-sided Students' T-tests ($p < 0.05$). The color intensity of each phage-host combination reflects the liquid assay score, which represents how well the phage strain can repress the growth of a given bacterial host. No inhibition of bacterial growth is reflected by a liquid assay score of 0, and complete suppression would result in a score of 100.

nature portfolio

Corresponding author(s): Joseph Bondy-Denomy

Last updated by author(s): Aug 3, 2022

Reporting Summary

Nature Portfolio wishes to improve the reproducibility of the work that we publish. This form provides structure for consistency and transparency in reporting. For further information on Nature Portfolio policies, see our Editorial Policies and the Editorial Policy Checklist.

Statistics

For all statistical analyses, confirm that the following items are present in the figure legend, table legend, main text, or Methods section.

n/a	Confirmed
☐	☒ The exact sample size (*n*) for each experimental group/condition, given as a discrete number and unit of measurement
☐	☒ A statement on whether measurements were taken from distinct samples or whether the same sample was measured repeatedly
☐	☒ The statistical test(s) used AND whether they are one- or two-sided *Only common tests should be described solely by name; describe more complex techniques in the Methods section.*
☒	☐ A description of all covariates tested
☒	☐ A description of any assumptions or corrections, such as tests of normality and adjustment for multiple comparisons
☐	☒ A full description of the statistical parameters including central tendency (e.g. means) or other basic estimates (e.g. regression coefficient) AND variation (e.g. standard deviation) or associated estimates of uncertainty (e.g. confidence intervals)
☐	☒ For null hypothesis testing, the test statistic (e.g. *F*, *t*, *r*) with confidence intervals, effect sizes, degrees of freedom and *P* value noted *Give P values as exact values whenever suitable.*
☒	☐ For Bayesian analysis, information on the choice of priors and Markov chain Monte Carlo settings
☒	☐ For hierarchical and complex designs, identification of the appropriate level for tests and full reporting of outcomes
☐	☒ Estimates of effect sizes (e.g. Cohen's *d*, Pearson's *r*), indicating how they were calculated

Our web collection on statistics for biologists contains articles on many of the points above.

Software and code

Policy information about availability of computer code

Data collection	NIS-Elements AR 5.02.00 64-bit, Image Lab (BioRad) software version 6.0.1, BioTek LogPhase 600 plate reader version 1.08, MiSeq Control Software version 3.1.0.13.
Data analysis	NIS-Elements AR 5.02.00 64-bit, Python 3.8, Geneious Prime® 2021.2.2. The custom python codes are available from public repositories at https://zenodo.org/record/6324407#.YiAjrejMI2w

For manuscripts utilizing custom algorithms or software that are central to the research but not yet described in published literature, software must be made available to editors and reviewers. We strongly encourage code deposition in a community repository (e.g. GitHub). See the Nature Portfolio guidelines for submitting code & software for further information.

Data

Policy information about availability of data

All manuscripts must include a data availability statement. This statement should provide the following information, where applicable:

- Accession codes, unique identifiers, or web links for publicly available datasets
- A description of any restrictions on data availability
- For clinical datasets or third party data, please ensure that the statement adheres to our policy

All relevant data are included in the paper and/or the Supplementary/Source Data files. The complete genome sequence of OMKO1 was deposited in GenBank under accession number ON631220. All strains and plasmids are available from the corresponding author upon request.

Field-specific reporting

Please select the one below that is the best fit for your research. If you are not sure, read the appropriate sections before making your selection.

☒ Life sciences ☐ Behavioural & social sciences ☐ Ecological, evolutionary & environmental sciences

For a reference copy of the document with all sections, see nature.com/documents/nr-reporting-summary-flat.pdf

Life sciences study design

All studies must disclose on these points even when the disclosure is negative.

Sample size	Sample sizes refer to the number of at least 500 bacterial cells in the dataset of each microscopic experiment.
Data exclusions	No data were excluded for analysis.
Replication	Plaque assays and time-lapse microscopic experiments were independently performed at least twice. Microplate liquid assays were performed in three independent replicates. One-step growth curves were independently performed at least three times.
Randomization	Randomization is not relevant to this work. The goal of this work is to develop a Cas13a-mediated genetic tool to engineer bacteriophages. It was sufficient to include an appropriate internal control (e.g. expression of a non-targeting Cas13a crRNA) and compare the effects with the gene-editing samples. In this respect, randomization is not necessary as we were investigating the possibility of Cas13-based genome editing in different bacteriophage strains.
Blinding	Blinding was not relevant in this study, as the effects of genome editing were individually tested by PCR or sequencing for each engineered phage strains.

Reporting for specific materials, systems and methods

We require information from authors about some types of materials, experimental systems and methods used in many studies. Here, indicate whether each material, system or method listed is relevant to your study. If you are not sure if a list item applies to your research, read the appropriate section before selecting a response.

Materials & experimental systems

n/a	Involved in the study
☒	☐ Antibodies
☒	☐ Eukaryotic cell lines
☒	☐ Palaeontology and archaeology
☒	☐ Animals and other organisms
☒	☐ Human research participants
☒	☐ Clinical data
☒	☐ Dual use research of concern

Methods

n/a	Involved in the study
☒	☐ ChIP-seq
☒	☐ Flow cytometry
☒	☐ MRI-based neuroimaging